Observational characteristics of pedestrian flows under high-density conditions based on controlled experiments

Cheng-Jie Jin[1,2], Rui Jiang[3,*], S.C. Wong[4,*], Siqi Xie[4], Dawei Li[1,2], Ning Guo[5], Wei Wang[1,2]

[1] *Jiangsu Key Laboratory of Urban ITS, Southeast University of China, Nanjing, Jiangsu 210096, China*

[2] *Jiangsu Province Collaborative Innovation Center of Modern Urban Traffic Technologies, Nanjing, Jiangsu 210096, China*

[3] *Key Laboratory of Transport Industry of Big Data Application Technologies for Comprehensive Transport, Ministry of Transport, Beijing Jiaotong University, Beijing 100044, China*

[4] *Department of Civil Engineering, The University of Hong Kong, Hong Kong SAR, China*

[5] *School of Automotive and Transportation Engineering, Hefei University of Technology, Hefei 230009, China*

Abstract

High-density crowds are associated with high risks such as stampede accidents. Therefore, it is important to understand the dynamics of high-density crowds. We performed experiments in both a 1.5-m-wide ring corridor and a single-file circular track to study pedestrian flow dynamics under high-density conditions. For the wide-track experiment, we examined global densities as high as 9 ped/m^2. Our main findings were as follows. (i) The middle section of our unidirectional fundamental diagram exhibited a clear similarity to that of a single-file pedestrian flow, which enabled us to distinguish two different kinds of congested pedestrian flow. (ii) The unidirectional fundamental diagram for a high-density situation was quantitatively nearly the same as that observed in the empirical data. (iii) In the absence of a bottleneck, typical stop-and-go patterns did not emerge in the unidirectional flow on the 1.5-m track. Instead, some high-density clusters propagating downstream can be observed. (iv) In the bidirectional flow experiments, three different lane formation processes were observed. The processes were quite quick, even under very dense conditions. (v) When three lanes formed, the bidirectional flow rate was much larger than the unidirectional flow rate due to the inhomogeneous distribution of pedestrians across different lanes. (vi) At high densities, the unidirectional and bidirectional flow rates were nearly the same. However, a bottleneck emerged in the bidirectional flow due to the variable width of the opposite streams. Our study helps to achieve a better understanding and modeling of the dynamics of high-density pedestrian flows.

Keywords: pedestrian flow; experiment; unidirectional flow; bidirectional flow; lane formation

[*] Corresponding authors. Email addresses: jiangrui@bjtu.edu.cn; hhecwsc@hku.hk.

1. Introduction

As the populations of major cities increase, large-scale events and activities that attract a very large number of people are becoming common, resulting in the formation of high-density crowds (Helbing, 2001; Hoogendoorn and Daamen, 2005; Duives et al., 2015; Ma and Yarlagadda, 2015; Haghani and Sarvi, 2018). Crowding, which reduces walking efficiency and can even threaten safety, is a key topic in pedestrian flow research. Crowd disasters can occur in places and events where there are high densities of pedestrian movements, such as religious pilgrimages and large entertainment events. Such disasters may include compressive asphyxiation, stampedes, and crushing and can lead to huge death tolls and serious injuries (Helbing et al., 2000; Gayathria et al., 2017). For example, crowd disasters are common in Mina/Makkah during the Hajj, where 1426 people were killed in 1990, 270 people in 1994, 118 people in 1998, 251 people in 2004, 345 people in 2006, and at least 2262 people in 2015. In 2010 in Duisburg, Germany, 21 people died and more than 500 people were injured in the crowd disaster during the Love Parade. In 2013, in Datia district, India, 115 people died in a temple stampede accident. In 2014, in Shanghai, China, a stampede accident killed 36 people and injured 42 people (Wikipedia, 2019). Therefore, a better understanding of the characteristics and behavior a high-density crowd is essential for the development of emerging technologies, such as advanced warning system and pedestrian navigation system, for crowd management and evacuation, which will help to reduce the risk of stampede in a crowd by eliminating the bottlenecks as far as possible.

Recent studies have identified super-high densities as a factor in crowd disasters. For example, densities as high as 10 ped/m^2 have been observed during the Hajj (Helbing et al., 2007; Johansson and Helbing, 2008). In the Love Parade disaster, the maximum density reached 11 ped/m^2 (Ma et al., 2013). As Helbing and Mukerji (2012) stated, “Once the crowd density exceeds between 4 or 5 persons per square meter, congestion can build up quickly, which implies high risks for people to stumble or fall. Therefore, injuries can easily happen.” Fruin (1993) pointed out that “at occupancies of about 7 persons per square meter the crowd becomes almost a fluid mass. People may be literally lifted out of their shoes, and have clothing torn off. Intense crowd pressures, exacerbated by anxiety, make it difficult to breathe, which may finally cause compressive asphyxia. The heat and the thermal insulation of surrounding bodies cause some to be weakened and faint.”

In order to model the crowd dynamics and better manage the crowd (Li et al., 2019; Haghani and Sarvi, 2019; Shiwakoti and Sarvi, 2013; Feng and Miller-Hooks, 2014; Chu et al., 2017), one needs to firstly understand the underlying mechanism. There are generally two approaches to studying crowd dynamics in crowd disasters: field observations and controlled experiments. The field observation approach is effective, as it is based on the actual behavior and characteristics of crowds during these events. However, detailed records of these disasters, such as video footage, are rare. Although some footage is available, most is not in the public domain or available to researchers. Furthermore, even when it is possible to access relevant footage, the low quality of these video records means that the level of detail is not sufficient for close analysis of the local crowd interactions and thus does not enable us to understand the crowd dynamics in disaster situations. Nevertheless, some useful attempts have made with important findings. Helbing et al. (2007) analyzed video recordings of the crowd disaster in

Mina/Makkah during the Hajj. They found two sequential, sudden transitions from laminar to stop-and-go and "turbulent" flows. They pointed out that stop-and-go patterns could be generated by coordination problems in bottleneck areas. Turbulence was also observed in the crowd disaster during the Love Parade, which was thought to be a consequence of amplifying feedback and cascading effects (Helbing and Mukerji, 2012). However, unlike the Hajj disaster, which happened under a unidirectional flow condition, the Love Parade disaster happened in a jammed crowd. Zhang et al. (2012b) studied crowd behavior during a mass event in which many people went through a door and then passed a bridge, and observed a laminar flow on the bridge and stop-and-go waves in the bottleneck area. The main disadvantages of the field observation approach are that it is extremely difficult, if not impossible, to plan the data collection process, such as video recording, as crowd disasters are rare events that are difficult to foresee. Moreover, these events are not repeatable, and thus it is difficult to neutralize the noise that blurs the relevant crowd behavior and thus extract the genuine characteristics and patterns.

An alternative approach is to conduct controlled experiments that reveal crowd dynamics and behavior. Numerous experiments have been performed to investigate unidirectional flow, bidirectional flow, and intersecting flow in circular corridor, open corridor, and intersecting corridor scenarios. However, as few of these studies have explored high-density crowds, and the maximum densities in the majority of these studies were not very great. A few experimental studies have looked at high-density situations. For example, Seyfried et al. (2009) studied pedestrian flows through bottlenecks of different widths. The maximum density in front of the bottleneck reached 7.5 ped/m^2. They found that maximal flow values measured at bottlenecks can significantly exceed the maxima predicted by empirical fundamental diagrams. Nicolas et al. (2017) studied the dynamics of pedestrian flows through a narrow doorway. They found that the flow rate grew monotonically with the local density ρ up to "close-packing" ($\rho \approx 9$ ped/m^2). Bode et al. (2019) found that in an experiment with four intersecting streams, the jams in some streams can coincide with higher flow rates in other streams, and the relative dominance of streams can switch stochastically. Lian et al. (2015) performed an experimental study of four-directional intersecting pedestrian flows. The test track had two corridors that intersected vertically. In that experiment, the maximum local density reached as high as 10 ped/m^2 in the cross-sectional area. The corresponding local flow rate was considerably larger than that observed in the case of the Hajj pilgrimage, perhaps because the cross-sectional area was very limited (3.2×3.2 m) and connected two low-density corridors.

Tables 1 and 2 summarize the maximum densities observed in previous field observation studies and controlled experiments. Clearly, there has been limited research on super-high density regimes, which is an important research gap, as understanding crowd dynamics and behavior at these densities is essential for predicting the occurrence of crowd disasters. To identify the underlying characteristics and patterns of crowds at super-high densities, we designed some controlled experiments to neutralize noise that might blur crowd behavior. Through these experiments, we were able to address the following research questions:

Table 1. Studies of density regimes using field observations

Reference	Scope	Maximum density (ped/m^2)
Morrall et al. (1991)	Public footpaths in a city	0.3
Rastogi et al. (2013)	Public footpaths in a city	1.2
Yao et al. (2012)	A transport terminal	1.5
Laxman et al. (2010)	Public footpaths in a city	1.6
Xie-Wong (2015)	Crosswalk in a city	1.9
Navin-Wheeler (1969)	Public footpaths in a city	2.2
Zhang et al. (2012b)	A small bridge	2.3
Bain-Bartolo (2019)	Starting line of Marathon	2.3
Oeding (1963)	Public footpaths in a city	2.7
Sutheerakul et al. (2017)	Public footpaths in a city	2.8
Gerilla (1995)	Public footpaths in a city	3.6
Sarsam (2013)	Public footpaths in a city	3.7
Older (1968)	Public footpaths in a city	4.5
Hankin-Wright (1958)	Subway stations	4.6
Weidmann (1993)	Average of 25 datasets	5.4
Tanaboriboon et al. (1986)	Public footpaths in a city	5.7
Mori-Tsukaguchi (1987)	Public footpaths in a city	6.1
Helbing et al. (2007)	Hajj site	10.0
Krausz-Bauckhage (2012) and Helbing-Mukerji (2012)	Open area for festival (Love Parade)	11.0

Table 2. Studies of density regimes using controlled experiments.

Reference	Scope	Maximum density (ped/m^2)	Density type
Moussaid et al. (2012)	Uni- and Bi-directional	1.2	Global
Suma et al. (2012)	Bi-directional	1.3	Global
Guo et al. (2016)	Uni- and Bi-directional	1.8	Local
Feliciani-Nishinari (2016)	Bi-directional	2.3	Local
Moussaid et al. (2011)	Bi-directional	2.3	Global
Plaue et al. (2011)	Intersecting	2.5	Local
Isobe et al. (2004)	Bi-directional	2.9	Global
Wong et al. (2010)	Intersecting	3.7	Local
Shi et al. (2016)	Intersecting	3.8	Local
Zhang et al. (2011, 2012a)	Bi-directional	4.0	Local
Daamen-Hoogendoorn (2003)	Bottleneck	4.5	Local
Feliciani-Nishinari (2018)	Intersecting	4.7	Global
Hankin-Wright (1958)	Uni-directional	5.4	Global
Shahhoseini-Sarvi (2019)	Intersecting	6.0	Local
Bode et al. (2019)	Intersecting	7.0	Local
Seyfried et al. (2009)	Bottleneck	7.5	Local

Nicolas et al. (2017)	Bottleneck	9.0	Local
Lian et al. (2015)	Intersecting	10.0	Local

(1) Do stop-and-go patterns appear in the absence of bottlenecks in high-density unidirectional flows? This question might have an important practical implication: Helbing et al. (2007) revealed that stop-and-go waves emerge in bottleneck areas, then transit into turbulent flows, which can lead to stampedes. If stop-and-go waves cannot emerge spontaneously in the absence of bottlenecks, then a potentially efficient way to prevent crowd disasters is to eliminate bottlenecks[1].

(2) What is the lane formation process in high-density bidirectional flows? Some stampede accidents (e.g., in Shanghai in 2014) have occurred in bidirectional flow regimes. It is well known that a significant feature of bidirectional flow is the lane formation process. Therefore, the questions arise of whether lanes form spontaneously in high-density bidirectional flows, and, if so, how they form, and how quickly they form. How might a crowd disaster be related to lane formation?

The controlled experiments covered both unidirectional and bidirectional pedestrian flows in high-density crowds of up to 9 ped/m^2. To study crowd behavior, we performed the experiment on one 1.5-m-wide ring corridor to avoid the boundary effect. The results revealed the dynamics of high-density pedestrian flow, which helps us to understand the operational characteristics of crowd movements, and thus sheds light on the occurrence of crowd disasters.

The rest of this paper is organized as follows. Section 2 describes the experiments. Sections 3 and 4 discuss the experimental results of the unidirectional and bidirectional flows, respectively. Section 5 concludes the paper.

2. Experimental setup

To study pedestrian dynamics in high-density situations, we conducted a pedestrian flow experiment on the Jiulonghu Campus of Southeast University, China. As real pedestrians are free to walk in a two-dimensional domain, to reveal the pedestrian dynamics of a high-density regime, we designed a wide-track experiment that mimicked a realistic walking environment.

To benchmark the results in the literature, we also performed a single-file experiment to reveal the longitudinal dynamics of pedestrian flow, in which pedestrians were required to walk in a narrow corridor and follow each other without overtaking (Seyfried et al., 2005; Chattaraj et al., 2009; Jelic et al., 2012a,b; Yanagisawa et al., 2012; Zhang et al., 2014; Cao et al., 2016; Zhao and Zhang, 2017). Seyfried et al. (2005) and Jelic et al. (2012b) used a linear transformation equation to compare the equivalence between single-file and wide-track pedestrian flows. Therefore, for comparison, we also performed a single-file experiment with a unidirectional flow.

The wide-track experiment was performed on Dec. 3, 2016 on a large square. It was a sunny day and there was nearly no wind. The single-file experiment was performed on Dec. 3,

[1] The bottleneck is known to induce arching phenomenon. When the arching forms, the flow rate decreases to very small value. When the arching is broken, the flow rate suddenly increases. The repeated formation and broken of arching leads to stop-and-go wave in high density crowd. Without a bottleneck, if the arching phenomenon does not emerge, the stop-and-go wave may be eliminated .

2017, on the same square. The weather was also good. The 278 and 203 student participants in the two experiments, respectively, were recruited through campus advertisements. The age of all of the participants was between 18 and 24, and the male to female ratio was about 1:1. Thus the experimental results are biased toward the behavior of young educated adults. For the wide-track experiment, plastic stools were used to define the boundaries, as shown in Fig. 1(a). The radius of the inner circle was 2 m, and that of the outer circle was 3.5 m. Therefore, the area of the ring corridor was approximately 26 m^2. For the single-file experiment, the radius of the circular track was 8 m, and the length of the track was approximately 50 m (see Fig. 1(b)). One of the advantages of using a circular track was that it maintained a continuous circulating flow throughout each scenario.

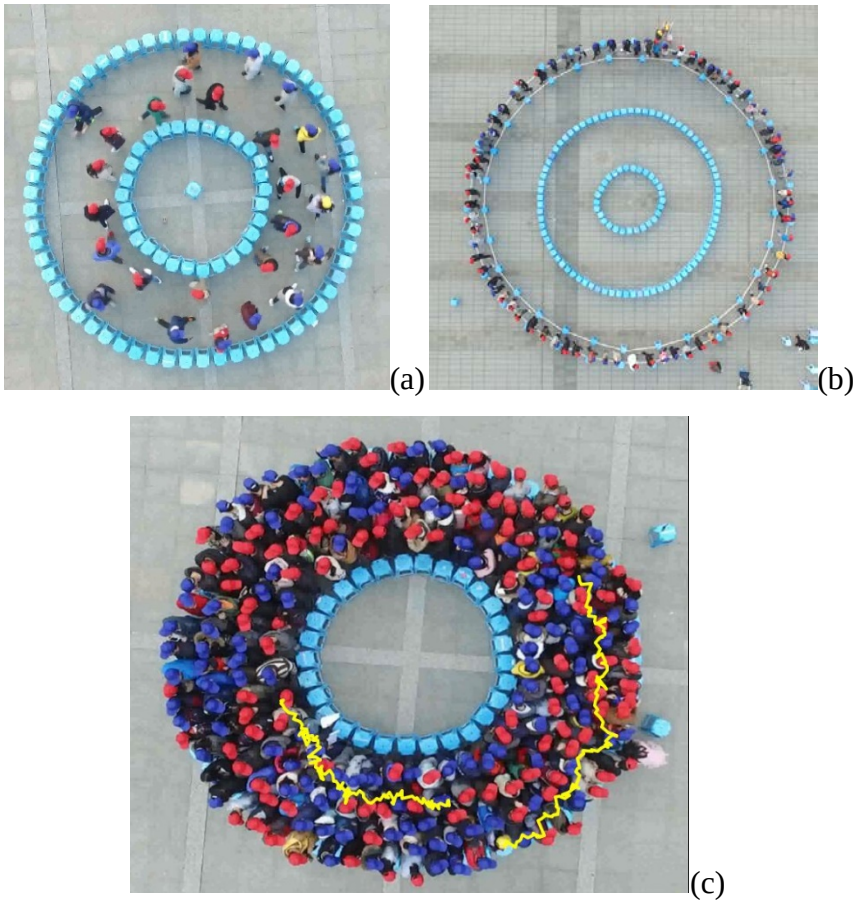

Fig. 1. Basic experimental configuration. (a) Uni- and bidirectional experiments in Run 1-1. (b) Single-file experiment in Run 1. (c) Two examples of pedestrian trajectories in unidirectional Run 9-1.

For both experiments, we used one unmanned aerial vehicle (UAV) to record the data. It hovered over the center of the two circles at a height of approximately 11.8 m in the wide-track experiment and 25.0 m in the single-file experiment. The video was taken at 30 frames per second at a resolution of 2704×1520. We used the *Tracker* (http://physlets.org/tracker/)

software to extract all of the data manually. The angle perpendicular to the camera was about 17° in the wide-track experiment and 18° in the single-file experiment. As Boltes et al. (2008) and Boltes et al. (2013) have discussed, when the height range of pedestrians is 40 cm (150 cm~190 cm), the corresponding errors in the measurements of the positions of pedestrians range from 12 cm to 13 cm. Fig.1(c) shows two examples of pedestrian trajectory in unidirectional Run 9-1, which might support the quality of the manual tracking.

In both experiments, we asked the participants in the low-density conditions to walk at a normal pace and the participants in the high-density conditions to move forward as far as they could. Before each run of the wide-track experiment, we first performed the unidirectional experiment. After a period of time, we asked the participants to stop. Then, to perform the bidirectional experiment, we asked the participants wearing blue caps to turn around. Although we were mainly interested in the high-density scenario, we also performed low-density experiments. Tables 3 and 4 show the details of each run in both experiments. The name of each run in Table 3 indicates the "predetermined density-order of the run." For instance, "8-2" means that the predetermined density of this second run was 8 ped/m^2. In the walking direction column "A" means anticlockwise and "C" means clockwise.

Table 3. Details of each run in the wide-track experiment

Run number	Actual density (ped/m^2)	Unidirectional experiment			Bidirectional experiment		
		Number of participants	Walk direction	Duration (min:sec)	Number of participants walking clockwise	Number of participants walking anticlockwise	Duration (min:sec)
9-1	9.04	235	A	7:40	117	118	9:40
8-1	7.69	200	A	4:28	101	99	5:05
7-1	6.27	163	A	4:39	78	85	4:11
6-1	5.65	147	A	2:32	70	77	4:06
5-1	4.85	126	A	2:00	65	61	2:03
9-2	8.35	217	C	3:51	106	111	2:21
8-2	7.65	199	C	2:31	100	99	3:23
7-2	6.42	167	C	2:19	84	83	4:10
6-2	5.69	148	C	1:50	74	74	2:09
5-2	4.73	123	C	1:48	59	64	2:10
4-1	4.04	105	C	1:29	53	52	1:39
3-1	3.19	83	C	1:06	41	42	1:08
2-1	2.15	56	C	1:07	28	28	1:02
1-1	1.00	26	C	1:01	13	13	0:53

Table 4. Details of each run in the single-file experiment

Run number	Actual density (ped/m)	Number of participants	Duration (min: sec)
1	1.41	71	4:51
2	2.15	108	5:29
3	2.43	122	4:36
4	3.02	152	4:49
5	3.58	180	5:52
6	4.04	203	8:48

3. Experimental results for unidirectional flow

3.1. Definitions of quantities measured

3.1.1 Wide-track experiment

To calculate local density, we divided the test track into eight[2] equal subareas, as shown in Fig. 2. We measured local density as follows:

$$\rho_l = \frac{N(t)+N(t+\Delta t)}{2\phi}. \quad (1)$$

This is an approximation of $\rho_l = \frac{1}{\phi}\int_t^{t+\Delta t} N(t)dt$, as defined by Zhang et al. (2011), where N(t) is the numbers of pedestrians in the subarea of size $\phi \approx 3.25\ m^2$ at time t. Δt was set to 15 s in this experiment[3]. Note that the total area of the wide-track was about $26\ m^2$, as shown in Figure 1a.

We measured the corresponding local flow rate as follows:

$$f_l = \frac{q}{W\Delta t}, \quad (2)$$

where q is the number of pedestrians who crossed the radial cross-section of the subarea and W refers to the width of the corridor (1.5 m).

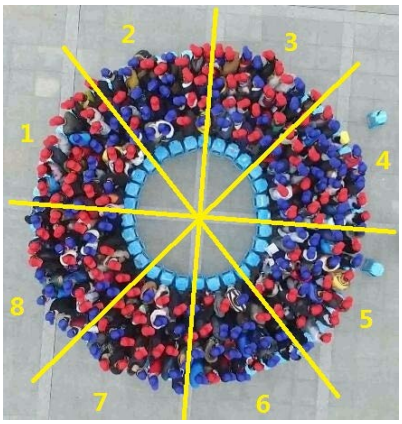

Fig. 2. Eight subareas. The snapshot is from Run 9-1.

[2] The results remained consistent when the number of subareas was varied between 6 and 10.
[3] The statistical results are rather robust when the time interval was varied between 10 s and 20 s.

3.1.2 Single-file experiment

In the single-file experiment, we also divided the track into eight equal parts (see Fig. 3). We measured the local flow rates as follows:

$$f_l = \frac{q}{\Delta t}, \tag{3}$$

and the local density as follows:

$$\rho_l = \frac{N(t)+N(t+\Delta t)}{2l}, \tag{4}$$

where N(t) is the number of pedestrians in a subsection of l = 6.28 m (one eighth of the perimeter of the ring track) at time t; Δt was set to 15 s in this experiment.

Fig. 3. The eight subareas in the single-file experiment.

3.2. Fundamental diagram

First, we investigated the fundamental diagrams of the unidirectional flow. As discussed in Zhang et al. (2011), there are different methods for defining the densities, but most require the measurement of the velocities of the pedestrians, see, e.g., Xiao et al. (2016). At high densities, the velocities are very low and thus the errors in the measurements are usually not small. Therefore, following Guo et al. (2016), we used a traditional area-based method to measure the densities and the cross-section method to measure the flow rate.

Fig. 4 shows the fundamental diagrams for both experiments. Two different coordination systems were used. The wide-track experimental results correspond to the bottom and left coordinate axis. The single-file experimental results correspond to the top and right coordinate axis. We averaged the local measure results over the density interval of 0.2 ped/m^2 for the wide-track experiment and 0.2 ped/m for the single-file experiment. Here we also show the raw data before averaging for the wide-track experiment in Fig.4(b), and the wide-scattered appearance could be clearly found.

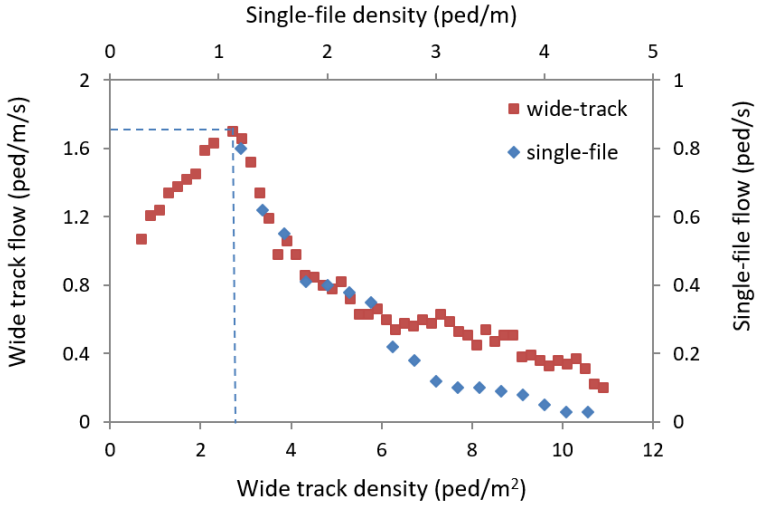

(a)

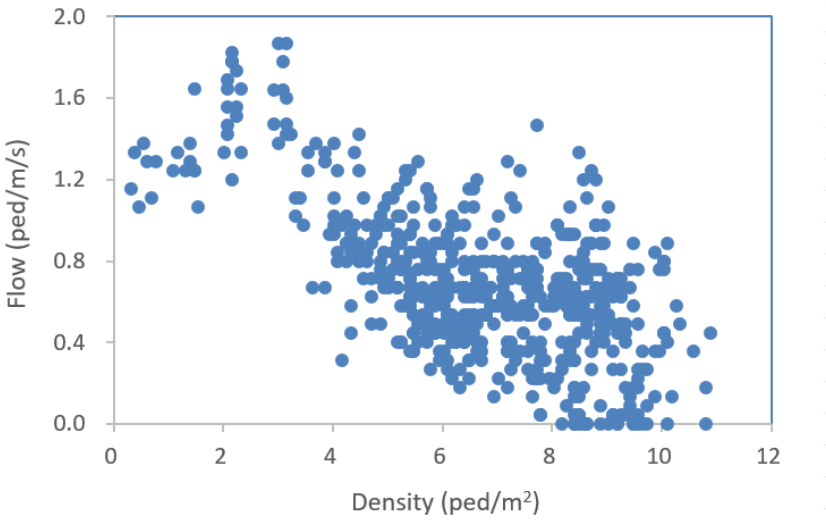

(b)

Fig. 4. Fundamental diagrams of the unidirectional pedestrian flow. (a) The averaged results in the two experiments. (b) The raw data of the wide-track experiments.

A critical density of $\rho_{c1} \approx 2.5$ ped/m^2 occurred in the wide-track experiment, where the maximum flow rate reached about 1.7 ped/m/s. The single-file experiment did not cover the low density regime, but, based on the literature, we anticipated that the critical density ρ'_{c1} was located within the density range between 0-1 ped/m (Jelic et al., 2012a; Cao et al., 2016).

A comparison of the decreasing branches in the fundamental diagrams of the two experiments revealed that they exhibited clear similarity when $\rho < \rho_{c2} \approx 6$ ped/m^2 in the wide-track experiment and $\rho < \rho'_{c2} \approx 2.5$ ped/m in the single-file experiment, showing a clear demarcation between the two density regimes. This finding enabled us to distinguish two kinds of congested pedestrian flow.

When $\rho < \rho_{c2}$ in the wide-track experiment and $\rho < \rho'_{c2}$ in the single-file experiment, there was essentially no body contact observed among the pedestrians. When $\rho > \rho_{c2}$ in the wide-track experiment and $\rho > \rho'_{c2}$ in the single-file experiment, body contact was inevitable and "physical force" played an important role. In this circumstance, the branch in the single-

file experiment was remarkably below that in the wide-track experiment. In the wide-track experiment, some lanes formed in the pedestrian flow.

When $\rho < \rho_{c2}$, only a small number of lanes formed (e.g., see Fig. 5(a) and (b), in which three lanes were formed) with limited interactions between adjacent lanes, as pedestrians tended to keep to their lanes when pedestrian speed was relatively high. As a result, the wide-track and single-file experiments exhibited clear similarities. However, when $\rho > \rho_{c2}$, the number of lanes in the wide-track experiment increased (e.g., see Fig. 5(c); 4 to 5 lanes formed), resulting in more interactions between pedestrian lanes, as pedestrians were tempted to change speed by changing lanes. Consequently, the similarity between the two regimes was broken, and the flow in the wide-track scenario decreased in a gentler manner than the flow in the single-file experiment in which there was no overtaking opportunity.

(a) (b) (c)

Fig. 5. Snapshots of the unidirectional experiment: (a) Run 3-1; (b) Run 5-1; and (c) Run 8-1.

3.3. Spatiotemporal evolution

We investigated the spatiotemporal evolution of local densities to determine whether we could observe stop-and-go waves. Nonlinear stop-and-go waves have been observed in many studies of pedestrian and vehicular flow and can be explained by the continuum theory (Hughes, 2002; Helbing et al., 2007). Nondamping linear waves were recently observed as marathon runners approached the starting line, which was also captured by a fluid-like model (Bain and Bartolo, 2019).

Fig. 6 shows typical spatiotemporal diagrams of the local densities in eight runs with high densities: 6-1, 6-2, 7-1, 7-2, 8-1, 8-2, 9-1, and 9-2. These figures show that typical stop-and-go waves do not emerge. In contrast, some high-density clusters propagate downstream, as marked by white arrows. They differ from the stop-and-go waves reported in previous studies, which usually propagated upstream. A comparison of the black and white arrows in Fig. 6 indicates that in each run, the moving speed of these high-density clusters is no less than that of the average pedestrians' speed. This implies that although pedestrians generally do not look backwards, they receive some "information" about the upstream conditions (i.e., behind them). This downstream transmission may be a result of pushing and physical contacts.

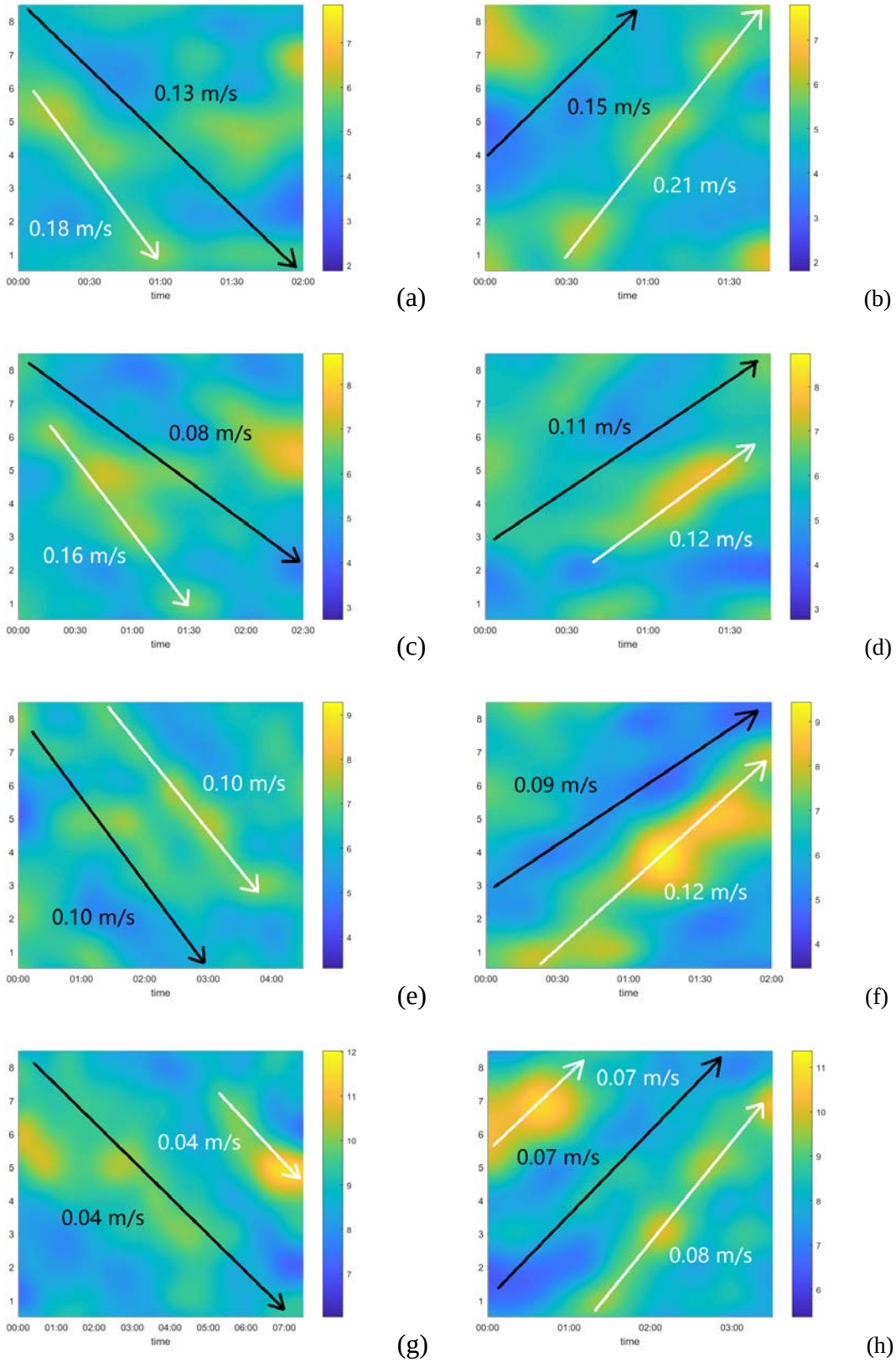

Fig. 6. Spatiotemporal diagrams of the local densities in unidirectional runs: (a) 6-1; (b) 6-2; (c) 7-1; (d) 7-2; (e) 8-1; (f) 8-2; (g) 9-1; and (h) 9-2. In Run 6-1/7-1/8-1/9-1 (6-2/7-2/8-2/9-2), the pedestrians walked counterclockwise (clockwise) from sub-area 8→7→ ⋯ →1→8 (1→2→⋯→8→1). White arrows indicate the propagation of high-density clusters, and black

arrows indicate the average pedestrians' speeds during this run.

However, in the single-file experiment, we observed stop-and-go waves in the intermediate density range (e.g., see Fig.7(a)), which is consistent with the results of many previous pedestrian experiments. Their average speed (about 0.4 m/s) was also similar to those found in previous papers. As the density increased, the high-density clusters also emerged and propagated downstream, albeit very slowly (~ 0.05 m/s), as shown in Fig.7(b). Nevertheless, the stop-and-go waves moving against the crowd remain visible, although they are less marked than the high-density clusters.

The failure of the stop-and-go waves to emerge in the wide-track experiment could be a result of the lateral movement of some pedestrians who try to avoid stopping by moving sideways. The difference between the inner radius and the outer radius may also have impeded the propagation of stop-and-go waves. In a future study, we will conduct further experiments to study the potential mechanisms.

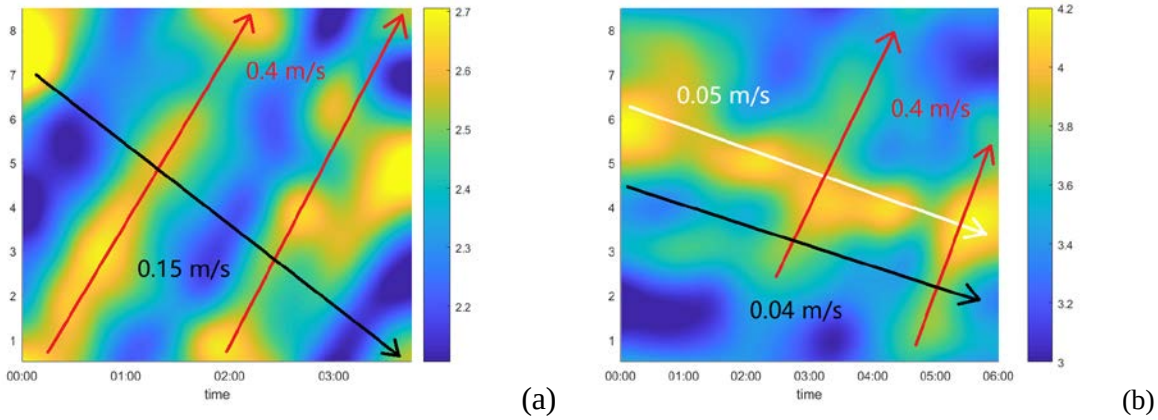

(a) (b)

Fig. 7. Spatiotemporal diagrams of local densities in the single-file experiment: (a) ρ=2.43 ped/m; (b) ρ=3.58 ped/m. The pedestrians walked counterclockwise from sub-areas 8→7→⋯ →1→8. Red arrows indicate stop-and-go waves, black arrows indicate the average pedestrians' speeds during this run, and white arrows indicate the propagation of high-density clusters.

3.4 Discussion

We compared our unidirectional data with the results of previous studies. First, we compared our unidirectional fundamental diagram with the empirical diagrams reported in previous studies (see Fig. 8). These data were obtained using different measurement methods, which may affect the fundamental diagrams. However, Zhang et al. (2011) found that for the same dataset, the averaged results of different methods were nearly the same, although the standard deviations were different. As Fig. 8 only displays the averaged flow rates, it is possible to compare the results of studies that used different methods.

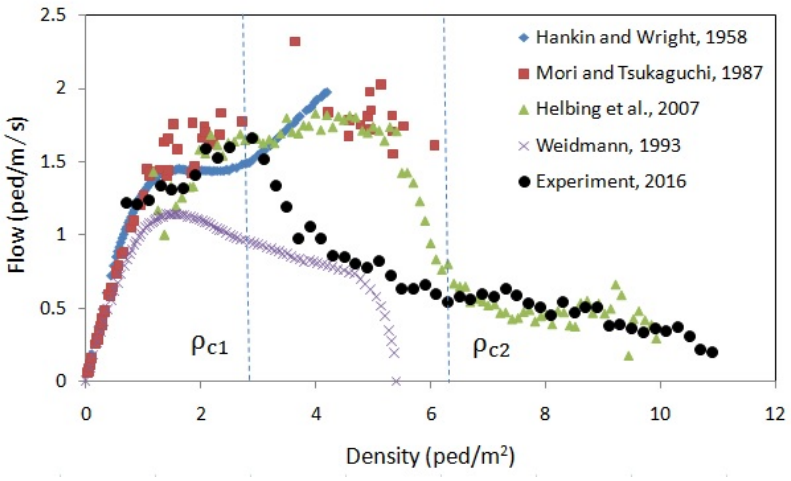

Fig. 8. Comparison of unidirectional data from our experiments and from other studies. The data were taken from www.asim.uni-wuppertal.de/en/database.html.

In this figure we observed the following.

(1) For low densities in the free flow state ($\rho < \rho_{c1}$), except for the data from Weidmann (1993), all of the studies had nearly the same results.

(2) For high densities ($\rho > \rho_{c2}$), our data were nearly quantitatively the same as those from Helbing et al. (2007), which confirmed the validity of our experiment. The high-density data were absent in the other studies, as the pedestrians did not feel comfortable with physical contact and chose to stop when the density approached ρ_{c2}. In fact, in the high-density situations where no instruction was given to move as far forward as they could, the participants in our experiment did not move.

(3) In the range $\rho_{c1} < \rho < \rho_{c2}$, the flow rate in our experiment was smaller than in Hankin-Wright (1958), Mori-Tsukaguchi (1987), and Helbing et al. (2007). We asked the participants to walk as usual when the density was not high. However, in Helbing et al. (2007), the pedestrians' walking behaviors were not normal; during the Hajj pilgrimage, the pedestrians hoped to walk as fast as possible. The data from Mori-Tsukaguchi (1987) were similar, as they were obtained from commuters, who usually walk fast to save time. The data from Hankin-Wright (1958) were collected from an experiment, but the instructions were not given in the paper. One possible reason for the difference is that the pedestrians were asked to move quickly.

However, the flow rate in Weidmann (1993) was lower than in our experiment, perhaps because Weidmann's data were the averaged values of 25 datasets. In some datasets, for example, the pedestrians might not have walked fast because they were shopping.[4]

4. Experimental results for bidirectional flow

Compared with the unidirectional pedestrian flow, a significant feature of the bidirectional flow was the lane formation process. Therefore, we discuss this process first, and then comment on the evolution process.

[4] The details of the 25 datasets were not provided in Weidmann's paper.

4.1. Lane formation process

We considered the lane formation process based on two indices: the average value ($\bar{r}_\omega(t)$) and standard deviation ($\sigma_{r,\omega}(t)$) of the radial positions of the pedestrians walking in the clockwise/anticlockwise direction at time instant t. The indices were defined as follows:

$$\bar{r}_\omega(t) = \frac{1}{N_\omega}\sum_{i=1}^{N_\omega} r_{\omega,i}(t) \quad (5)$$

$$\sigma_{r,\omega}(t) = \frac{1}{N_\omega - 1}\sum_{i=1}^{N_\omega}\left(r_{\omega,i}(t) - \bar{r}_\omega(t)\right)^2. \quad (6)$$

Here, ω denotes the walking direction (clockwise or anticlockwise), N_ω refers to the number of participants walking in direction ω, and $r_{\omega,i}(t)$ is the radial location of participant i walking in direction ω at time instant t.

In our experiment, the numbers of participants walking in the two directions were roughly the same. In each run, either two or three lanes were formed. Therefore, we used the two indices to quantify the lane formation. When the participants separated into two lanes, the $\bar{r}_\omega$ value of the participants in the outer lane was remarkably larger than in the inner lane. When the participants separated into three lanes, the $\bar{r}_\omega$ values of the two directions were roughly equal. However, the $\sigma_{r,\omega}$ value in the middle lane was remarkably smaller than those in the outer and inner lanes.

Fig. 9 shows three typical lane formation processes. Here, C denotes the results for the clockwise-moving pedestrians, and A represents those of the anticlockwise-moving pedestrians. Fig. 9(a) shows the first process (Run 9-1), in which $\sigma_{r,\omega}$ increased remarkably in one direction and decreased in the other direction. For the former direction, the pedestrians split into one inner lane and one outer lane. For the latter direction, the pedestrians gathered into the middle lane. Fig. 10 shows one snapshot at T=0:43 in Run 9-1, where the three lanes were formed.

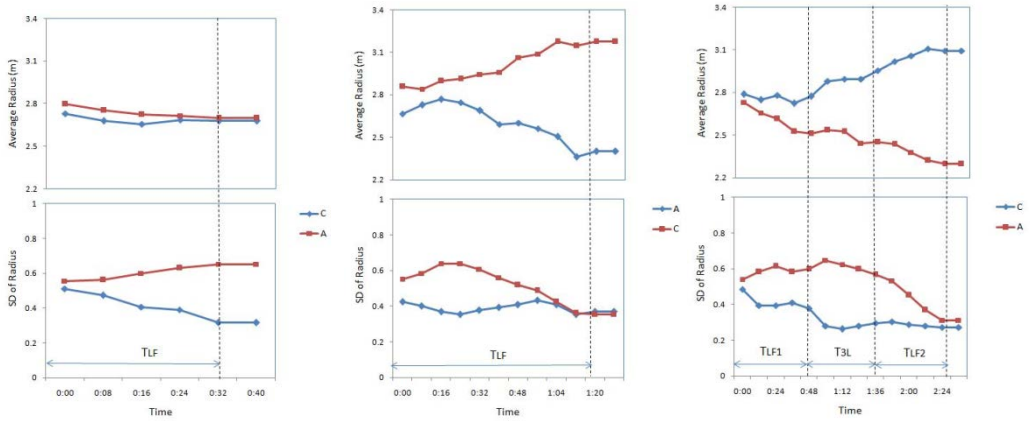

(a) (b) (c)

Fig. 9. Evolution of pedestrian radii during the lane formation process: (a) bidirectional Run 9-1; (b) bidirectional Run 8-2; and (c) bidirectional Run 8-1.

Fig. 10. Video snapshot of the lane formation process in bidirectional Run 9-1, T=0:43.

Fig. 9(b) shows the second process (Run 8-2), in which $\bar{r}_{\omega}$ increased in one direction and decreased in the other direction. In the former/latter direction, pedestrians gathered in the outer/inner lane. Although it varied remarkably during the lane formation process, $\sigma_{r,\omega}$ became almost equal in the two directions once the two lanes were formed. Fig. 11 shows a snapshot at T=1:17 in Run 8-2 when the two lanes were formed.

Fig. 11. Video snapshot of the lane formation process in bidirectional Run 8-2, T=1:17.

Fig. 9(c) shows the third process (Run 8-1), in which the lane formation process could be classified into two sub-processes. In the first sub-process, three lanes formed, similar to the case shown in Fig. 10. The three lanes were maintained for a certain interval (see Fig. 12(a), the yellow-circled pedestrian is the leader of the outer lane). At the beginning of the second sub-process, a gap appeared in the middle lane. The leading pedestrian of the outer lane crossed the middle lane through the gap (see the yellow-circled pedestrian in Fig. 12(b)), and the other pedestrians followed the leader and crossed the lane as well. As a result, the three lanes eventually transited into two lanes (see Fig. 12(c)).

(a) (b) (c)

Fig. 12. Video snapshots of the lane formation process in bidirectional Run 8-1: (a) T=0:48; (b) T=1:36; and (c) T=2:28.

For the first and second types of process, we studied the lane formation time (denoted by T_{LF}). For the third type of process, we studied the lane formation time of the two sub-processes (denoted by T_{LF1} and T_{LF2}, respectively) and the duration of the temporary three-lane state (T_{3L}). Table 5 shows that the formation of three lanes was usually quick, even at very high densities. The longest time was approximately 48 s in the first sub-process in Run 8-1. However, at high densities, the direct formation of the two lanes took longer (e.g., approximately 78 s in Run 8-2) due to temporary congestion. Moreover, the durations of the three-lane state fluctuated significantly. For example, it lasted for 116 s in Run 7-2, but was maintained for only 13 s in Run 6-2. In addition, when the system width increased, more than three lanes could form. This phenomenon will be studied in future experiments.

Table 5. Lane formation processes of all of the bidirectional runs

Type of processes	Run number	T_{LF} (s)	T_{LF1} (s)	T_{3L} (s)	T_{LF2} (s)
1	9-1	42	/	/	/
	9-2	28	/	/	/
	6-1	18	/	/	/
	5-2	15	/	/	/
2	8-2	78	/	/	/
	5-1	29	/	/	/
	3-1	18	/	/	/
	2-1	14	/	/	/
	1-1	4	/	/	/
3	8-1	/	48	48	52
	7-1	/	30	82	16
	7-2	/	35	116	21
	6-2	/	22	13	15
	4-1	/	11	8	24

4.2. Evolution after lane formation

4.2.1. Fundamental diagram

We also considered the evolution of the flows after the lane formation processes. Fig. 13(a) plots the local measurement results of the bidirectional fundamental diagram and compares them with those of the unidirectional experiment. Here the flow rate in bidirectional pedestrian flow equals to the sum of flow rates in both directions. We classified the density ranges into four categories.

When the density was very high ($\rho > \rho''_{c3}$), the bidirectional and unidirectional flow rates were roughly equal. In the density range $\rho''_{c2} < \rho < \rho''_{c3}$, the bidirectional flow rate was larger than the unidirectional flow rate. In the density range $\rho''_{c1} < \rho < \rho''_{c2}$, the bidirectional flow rate was lower than the unidirectional flow rate. Finally, in the free flow ($\rho < \rho''_{c1}$), almost no interaction was observed between the pedestrians. Thus, the bidirectional and unidirectional flow rates were equal.

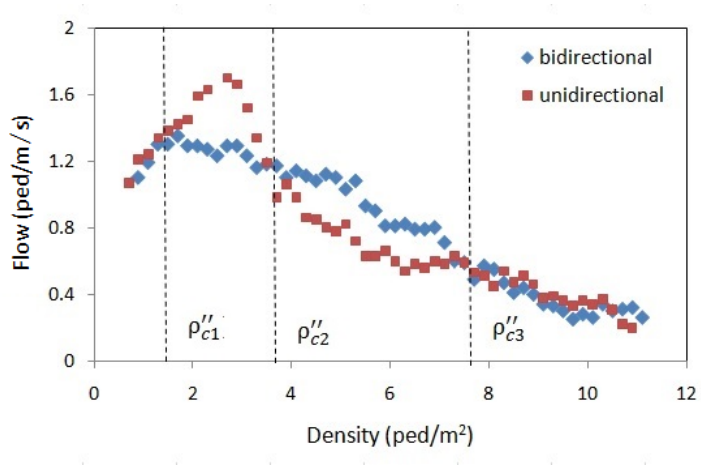

(a)

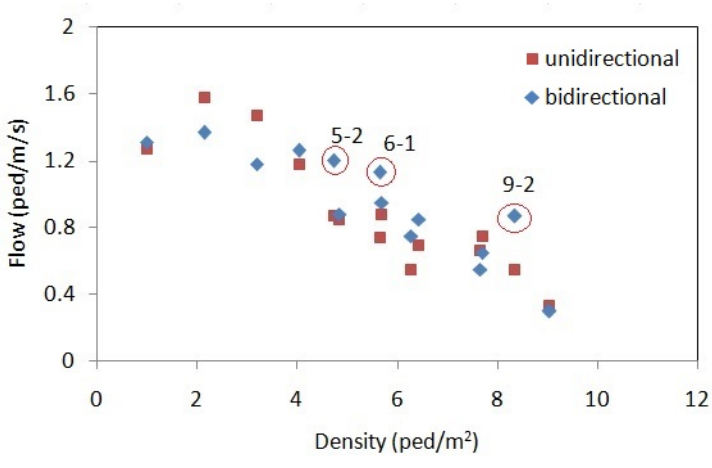

(b)

Fig.13. Bidirectional fundamental diagrams: (a) Local measurements; and (b) Global measurements.

Fig. 13(b) shows the global measurements of the bidirectional fundamental diagram and compares them with those of the unidirectional experiment. Here, global flow was calculated

as the average of the local flow rates over time and over the eight cross-sections. The bidirectional flow rates were remarkably larger than the unidirectional flow rates in Runs 5-2, 6-1, and 9-2 (indicated by the red circles). For the other runs, the bidirectional flow rates were close to or even smaller than the unidirectional flow rates. Three lanes formed in Runs 5-2, 6-1, and 9-2, and two lanes formed in the other runs, indicating that the formation of more than two lanes could play a nontrivial role in bidirectional pedestrian dynamics. To further illustrate the issue, we investigated the evolution process of pedestrian flow.

4.2.2. Evolution process

(1) When the density was below ρ_{c2}'', the evolution process was simple. The pedestrians self-organized into two lanes quickly. The distribution of pedestrians was rather homogeneous (e.g., see Fig. 14).

Fig. 14. Video snapshot after the lane formation process in bidirectional Run 2-1, T=0:40.

(2) In Run 4-1, the global density was in the vicinity of ρ_{c2}''. The localized crowd formed and dissipated; see the typical snapshots in Fig. 15. At T=0:51, some pedestrians formed a localized crowd on the right side (see Fig. 15(a)). In contrast, the density on the left side was very low. The localized crowd basically disappeared at T=1:13 (see Fig. 15(b)), but emerged again at T=1:32 (see Fig. 15(c)). In both directions, the average lane width was between 1 and 2; the lane width equaled 1 in some places and 2 elsewhere. In general, when one two-file stream met another two-file stream in the opposite direction, a localized crowd emerged.

(a) (b) (c)

Fig. 15. Video snapshots after the lane formation process in bidirectional Run 4-1: (a) T=0:51; (b) T=1:13; and (c) T=1:32.

(3) When the density exceeded ρ''_{c2} and three lanes were formed, an inhomogeneous distribution of pedestrians between different lanes sometimes occurred. Fig. 16(a) shows the three lanes that formed in Run 6-1. After the lane formation, the pedestrian densities of the inner and outer lanes were significantly different. Although the inner lane was much less dense, pedestrians in the middle lane did not invade the space of the inner lane. As a result, the flow rate of the inner lane was approximately 0.88 ped/s, considerably higher than that of the outer lane (approximately 0.22 ped/s). In this circumstance, the high flow of the inner lane contributed significantly to the large average flow rate of the bidirectional flow.

Fig. 16(b) shows a snapshot of Run 5-2. A similar phenomenon was observed: the distribution of red pedestrians was also inhomogeneous, and the density of the outer lane was much lower. As a result, the flow rate was approximately 0.23 ped/s in the inner lane and 0.46 ped/s in the outer lane. In this situation, the high flow of the outer lane led to a large averaged flow rate.

Fig. 16(c) shows a snapshot of Run 9-2. The density of the inner lane was obviously smaller than that of the outer lane. The flow rate of the inner lane (approximately 0.28 ped/s) was also much higher than that of the outer lane (approximately 0.06 ped/s). As a result, the average flow rate was remarkably large.

(a) (b) (c)

Fig. 16. Video snapshots after the lane formation process when three lanes were formed: (a) bidirectional Run 6-1, T=1:10; (b) bidirectional Run 5-2, T=1:20; and (c) bidirectional Run 9-2, T=1:00.

(4) When the density was very large, pedestrian movement was difficult. In this circumstance, bottlenecks sometimes emerged. For example, in Run 9-1, after the lane formation, a large group of pedestrians wearing red caps gathered together, which formed a bottleneck. As a result, the local density was higher in front of the bottleneck, as indicated by region marked with the yellow line in Fig. 17(a) ($\rho \approx 9.8$ ped/m^2). Outside this region, the local density was lower ($\rho \approx 8.4$ ped/m^2). The bottleneck was essentially stuck due to the high density, as indicated by Fig. 17(b), in which $\rho \approx 10.2$ ped/m^2 in the yellow region and $\rho \approx 8.5$ ped/m^2 outside the region. The bottleneck gradually became weaker and basically disappeared at the end of this run (see Fig. 17(c)). The formation of the bottleneck might be the origin of crowd disasters in high-density bidirectional flows.

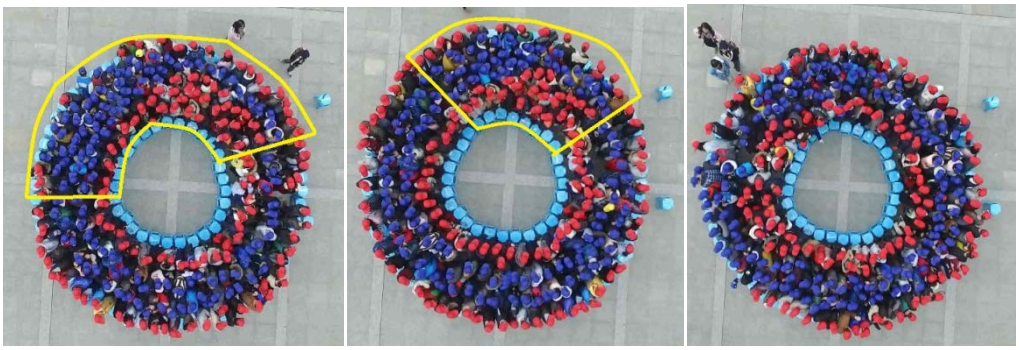

(a) (b) (c)

Fig. 17. Video snapshots after the lane formation process in bidirectional Run 9-1: (a) T=2:00; (b) T=5:00; and (c) T=9:40.

4.3. Discussion

We compared our bidirectional data with those of previous studies. Table 6 shows the setups of some previous bidirectional experiments. In the previous studies, all of the maximum densities were low. In those with open boundary conditions, the maximum value was 4 ped/m^2, whereas in those with periodic boundary conditions, the maximum value was no more than 2 ped/m^2. In all of the experiments, pedestrian lanes formed quickly. For example, in the experiment conducted by Moussaid et al. (2012), two lanes formed within 10 s at a global density of $\rho = 1.2$ ped/m^2. In the experiment conducted by Guo et al. (2016), two lanes also formed after about 10 s at a global density of $\rho = 1.3$ ped/m^2. Both results were qualitatively the same as our experimental results.

Table 6. Setups of some previous bidirectional experiments

Experiment	Country	Boundary condition	Corridor width (m)	Maximum density (ped/m^2)
Moussaid et al. (2012)	France	Periodic	2.5	1.2
Guo et al. (2016)	China	Periodic	3.0	1.8
Suma et al. (2012)	Japan	Open	3.0	1.3
Moussaid et al. (2011)	France	Open	1.8	2.3

Feliciani-Nishinari (2016)	Japan	Open	3.0	2.3
Isobe et al. (2004)	Japan	Open	2.0	2.9
Zhang et al. (2011, 2012a)	Germany	Open	3.0, 3.6	4.0

We compared our bidirectional fundamental diagram with the data collected in previous studies (see Fig. 18). Similar to Fig. 8, the data points were the averaged values of the raw data, and the density interval was 0.2 ped/m^2. As in the previous case, data at high densities were lacking, but we could compare the results at low densities. In the free flow ($\rho < \rho''_{c1}$), the flow rates in our experiment were close to those in Older (1968) and Navin-Wheeler (1969). However, when $\rho''_{c1} < \rho < \rho''_{c2}$, the flow rates in our experiment were much higher, for two potential reasons. The first is different walking styles. For example, Older (1968) obtained data from shopping streets, where people may walk slowly. The second reason is that we collected the flow rates in our experiment after lane formation. Thus, the interactions between opposing streams had become weaker by the time we started collecting data.

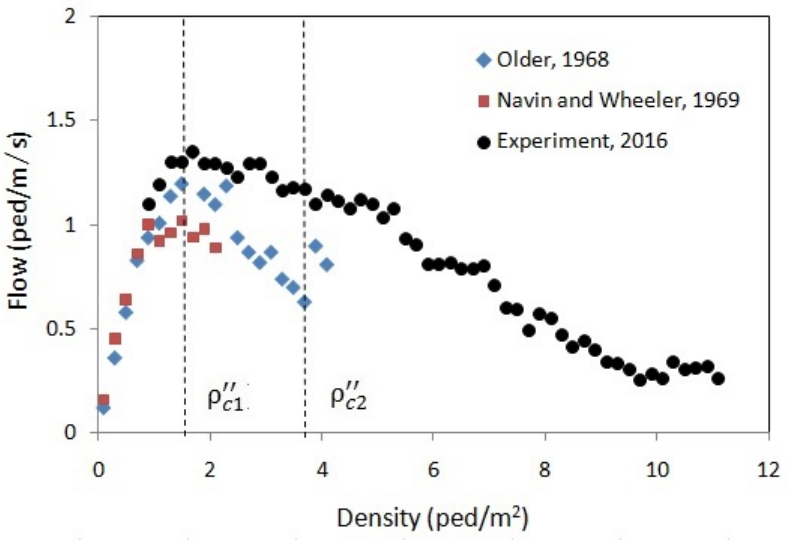

Fig. 18. Comparison between our experimental results and other studies of bidirectional data. The raw data from Older (1968) and Navin-Wheeler (1969) were taken from the www.asim.uni-wuppertal.de/en/database.html.

Finally, Zhang et al. (2012a) compared the fundamental diagrams of unidirectional and bidirectional flows and found similar phenomena. When $\rho < 1$ ped/m^2, the bidirectional and unidirectional flow rates were equal. When 1 ped/m^2 $< \rho <$ 3 ped/m^2, the unidirectional flow rates were higher than the bidirectional flow rates. As the authors explained, the interactions between opposing streams remained relevant, although the self-organized lanes could decrease head-on conflicts. When $\rho > 3$ ped/m^2, the bidirectional flow rates increased. However, the maximum density in these experiments was only about 4 ped/m^2. Thus, they did not find that the bidirectional flow rate became equal to the unidirectional flow rate again at very high densities.

5. Conclusions

The aim of this study was to improve the safety of pedestrians in high-density crowds, where stampede accidents are prone to occur. Our high-density experiment in a 1.5-m-wide circular corridor had three goals: (i) to investigate the fundamental diagram of a high-density pedestrian flow; (ii) to determine whether a stop-and-go pattern could be observed in a unidirectional flow in the absence of a bottleneck; and (iii) to study the lane formation phenomenon in a bidirectional flow.

For the unidirectional flow experiments, we developed a fundamental diagram. A comparative analysis showed that its middle section exhibited a clear similarity to that of a single-file pedestrian flow. This finding enabled us to distinguish two different kinds of congested pedestrian flow. The comparison showed that the fundamental diagram in a high-density situation was nearly quantitatively the same as that observed in the empirical data. Our analysis of the spatiotemporal evolution showed that in the absence of a bottleneck, typical stop-and-go waves did not emerge in the unidirectional flow in a 1.5-m track. Instead, some high-density clusters emerge, which propagate downstream but are almost still in the pedestrians' co-moving frame.

In the bidirectional flow experiments, three different types of lane formation processes were observed: (1) three lanes were directly formed; (2) two lanes were directly formed; and (3) three lanes were formed and then transited into two lanes. The lane formation process was quite quick, even under very dense conditions. When three lanes were formed, the bidirectional flow rate was remarkably larger than the unidirectional flow rate due to the inhomogeneous distribution of the pedestrians across different lanes. At high densities, the unidirectional and bidirectional flow rates were nearly the same. However, a pedestrian bottleneck emerged in the bidirectional flow due to the variable width of the opposite streams.

Our results should help to inform pedestrian dynamics and establish pedestrian flow modeling at high densities. Nevertheless, since our experimental data remain limited, more large-scale experiments involving larger numbers of participants are needed, and different configurations should be considered in the future.

Acknowledgments

We express our sincere gratitude to Xue Jin, Zi-Xin Wu, Jin-Lian Wu, Jun-Lan Chen, Wei Wei, Ming-Zhe Zang, Jun-Lin Yin, Yang Zhao, Ling-Yu Meng, Xiao-Bo Dong, Tian-Shu Wang, Ling-Hui Li, Rui-Wen Li, Hui-Jie Song, and Qi-qi Zhou for their help in extracting the data from the experimental video. This work was supported by the National Key R&D Program of China (No. 2017YFC0803300), National Natural Science Foundation of China (Nos. 71931002, 51608115, 71621001, 71801036), and the Research Grants Council of the Hong Kong Special Administrative Region, China (No. 17201318). The third author was also supported by the Francis S Y Bong Professorship in Engineering.

References

Bain, N., Bartolo, D., 2019. Dynamic response and hydrodynamics of polarized crowds. Science 363, 46–49.

Bode, N. W. F., Chraibi, M., Holl, S., 2019. The emergence of macroscopic interactions between intersecting pedestrian streams. Transportation Research Part B 119, 197-210.

Boltes, M., Seyfried, A., 2013. Collecting pedestrian trajectories. Neurocomputing 100, 127–133

Boltes, M., Seyfried, A., Steffen, B., Schadschneider, A., 2008. Automatic extraction of pedestrian trajectories from video recordings. Pedestrian and Evacuation Dynamics 2008, pp. 43-54.

Cao, S., Zhang, J., Salden, D., Ma, J., Shi, C., Zhang, R., 2016. Pedestrian dynamics in single-file movement of crowd with different age compositions. Physical Review E 94, 012312.

Chattaraj, U., Seyfried, A., Chakroborty, P., 2009. Comparison of pedestrian fundamental diagram across cultures. Advances in Complex Systems 12, 393.

Chu, J. C., Chen, A. Y., Lin, Y.-F., 2017. Variable guidance for pedestrian evacuation considering congestion, hazard, and compliance behavior. Transportation Research Part C 85, 664-683.

Daamen, W., Hoogendoorn, S. P., 2003. Controlled experiments to derive walking behaviour. European Journal of Transport and Infrastructure Research 3, 39-59.

Duives, D. C., Daamen, W., Hoogendoorn, S. P., 2015. Quantification of the level of crowdedness for pedestrian movements. Physica A 427, 162-180.

Feliciani, C., Nishinari, K., 2016. Empirical analysis of the lane formation process in bidirectional pedestrian flow. Physical Review E 94, 032304.

Feliciani, C., Nishinari, K., 2018. Measurement of congestion and intrinsic risk in pedestrian crowds. Transportation Research Part C 91, 124-155.

Feng L, Miller-Hooks E, 2014. A network optimization-based approach for crowd management in large public gatherings. Transportation Research Part C: Emerging Technologies, 42, 182-199.Furin, J. J., 1993. The causes and prevention of crowd disasters. The First International Conference on Engineering for Crowd Safety, London, England, pp. 1-10.

Gayathria, H., Aparnaa, P. M., Verma, A., 2017. A review of studies on understanding crowd dynamics in the context of crowd safety in mass religious gatherings. International Journal of Disaster Risk Reduction 25, 82-91.

Gerilla, G. P., 1995. Proposed level of service standards for walkways in metro Manila. Journal of the Eastern Asia Society for Transportation Studies 1, 1041-1060.

Guo, N., Hao, Q. Y., Jiang, R., Hu, M. B., Jia, B., 2016. Uni- and bi-directional pedestrian flow in the view-limited condition: Experiments and modeling. Transportation Research Part C 71, 63-85.

Haghani, M., Sarvi, M., 2018. Crowd behaviour and motion: Empirical methods. Transportation Research Part B 107, 253-294.

Haghani, M., Sarvi, M., 2019. Simulating dynamics of adaptive exit-choice changing in crowd evacuations: Model implementation and behavioural interpretations. Transportation Research Part C: Emerging Technologies, 103, 56-82.

Hankin, B. D., Wright, R. A., 1958. Passenger flow in subways. Operation Research Quarterly

9, 81-88.
Helbing, D., 2001. Traffic and related self-driven many-particle systems. Review of Modern Physics 73, 1067-1141.
Helbing, D., Mukerji, P., 2012. Crowd disasters as systemic failures: Analysis of the Love Parade disaster. EPJ Data Science 1, 7.
Helbing, D., Farkas, I., Vicsek, T., 2000. Simulating dynamical features of escape panic. Nature 407, 487-490.
Helbing, D., Johansson, A., Al-Abideen, H., 2007. Dynamics of crowd disasters: An empirical study. Physical Review E 75, 046109.
Hoogendoorn, S. P., Daamen, W., 2005. Pedestrian behavior at bottlenecks. Transportation Science 39, 147-159.
Hughes, R. L., 2002. A continuum theory for the flow of pedestrians. Transportation Research Part B 36, 507-535.
Isobe, M., Adachi, T., Nagatani, T., 2004. Experiment and simulation of pedestrian counter flow. Physica A 336, 638-650.
Jelic, A., Appert-Rolland, C., Lemercier, S., Pettré, J., 2012a. Properties of pedestrians walking in line: Fundamental diagrams. Physical Review E 85, 036111.
Jelic, A., Appert-Rolland, C., Lemercier, S., Pettré, J., 2012b. Properties of pedestrians walking in line. II. Stepping behavior. Physical Review E 86, 046111.
Johansson, A., Helbing, D., 2008. From crowd dynamics to crowd safety: a video-based analysis. Advances in Complex Systems, 11, 497-527.
Krausz, B., Bauckhage, C., 2012. Love Parade 2010: Automatic video analysis of a crowd disaster. Computer Vision and Image Understanding 116, 307-319.
Laxman, K. K., Rastogi, R., Chandra, S., 2010. Pedestrian flow characteristics in mixed traffic conditions. Journal of Urban Planning and Development, 136, 23-33.
Li L, Liu H, Han Y, 2019. Arch formation-based congestion alleviation for crowd evacuation. Transportation Research Part C: Emerging Technologies, 100, 88-106.
Lian, L., Mai, X., Song, W., Yuen, R. K. K., Wei, X., Ma, J., 2015. An experimental study on four-directional intersecting pedestrian flows. Journal of Statistical Mechanics P08024.
Ma, W., Yarlagadda, P. K. D. V., 2015. Pedestrian dynamics in real and simulated world. Journal of Urban Planning and Development 141, 04014030.
Ma, J., Song, W. G., Lo, S. M., Fang, Z. M., 2013. New insights into turbulent pedestrian movement pattern in crowd-quakes. Journal of Statistical Mechanics P02028.
Mori, M., Tsukaguchi, H., 1987. A new method for evaluation of level of service in pedestrian facilities. Transportation Research Part A 21, 223-234.
Morrall, J. F., Ratnayake, L. L., Seneviratne, P. N., 1991. Comparison of central business district pedestrian characteristics in Canada and Sri Lanka. Transportation Research Record 1294, 57-61.
Moussaïd, M., Helbing, D., Theraulaza, G., 2011. How simple rules determine pedestrian behavior and crowd disasters. Proceedings of the National Academy of Sciences 108, 6884-6888.
Moussaïd, M., Guillot, E. G., Moreau, M., Fehrenback, J., Chabiron O., Lemercier, S., Pettré, J., Appert-Rolland, C., Degond, P., Theraulaz, G., 2012. Traffic instabilities in self-organized pedestrian crowds. PLOS Computational Biology 8, e1002442.

Navin, P., Wheeler, R., 1969. Pedestrian flow characteristics. Traffic Engineering 19, 30-33.
Nicolas, A., Bouzat, S., Kuperman, M. N., 2017. Pedestrian flows through a narrow doorway: Effect of individual behaviours on the global flow and microscopic dynamics. Transportation Research Part B 99, 30-43.
Oeding, D., 1963. Verkehrsbelastung und Dimensionierung von Gehwegen und anderen Anlagen des FußgängerverkehrsStraßenbau und Straßenverkehrstechnik, Heft 22, in German.
Older, S., 1968. Movement of pedestrians on footways in shopping streets. Traffic Engineering and Control 10, 160-163.
Plaue, M., Chen, M., Bärwolff, G., Schwandt, H., 2011. Trajectory extraction and density analysis of intersecting pedestrian flows from video recordings. Proceedings of the 2011 ISPRS Conference on Photogrammetric Image Analysis, Berlin, pp. 285-296.
Rastogi, R., Ilango, T., Chandra, S., 2013. Pedestrian flow characteristics for different pedestrian facilities and situations. European Transport 53, paper 5.
Sarsam, S. I., 2013. Assessing pedestrian flow characteristics at Baghdad CBD area. 2nd Scientific Engineering Conference, University of Mosul: pp. 19-21.
Seyfried, A., Steffen, B., Klingsch, W., Boltes, M., 2005. The fundamental diagram of pedestrian movement revisited. Journal of Statistical Mechanics, P10002.
Seyfried, A., Steffen, B., Winkens, A., Rupprecht, T., Boltes, M., Klingsch, W., 2009. Empirical data for pedestrian flow through bottlenecks. Traffic and Granular Flow 2007, pp. 189-199.
Shiwakoti N, Sarvi M, 2013. Enhancing the panic escape of crowd through architectural design. Transportation Research Part C: Emerging Technologies, 37, 260-267.Shahhoseini, Z., Sarvi, M., 2019. Pedestrian crowd flows in shared spaces: Investigating the impact of geometry based on micro and macro scale measures. Transportation Research Part B, 122, 57-87.
Shi, X., Ye, Z., Shiwakoti, N., Tang, D., Wang, C., Wang, W., 2016. Empirical investigation on safety constraints of merging pedestrian crowd through macroscopic and microscopic analysis. Accident Analysis and Prevention, 95: 405-416.
Suma, Y., Yanagisawa, D., Nishinari, K., 2012. Anticipation effect in pedestrian dynamics: Modeling and experiments. Physica A 391, 248-263.
Sutheerakul, C., Kronprasert, N., Kaewmoracharoen, M., Pichayapan, P., 2017. Application of unmanned aerial vehicles to pedestrian traffic monitoring and management for shopping streets. Transportation Research Procedia 25, pp. 1717-1734.
Tanaboriboon, Y., Hwa, S. S., Chor, C. H., 1986. Pedestrian characteristics study in Singapore. Journal of Transportation Engineering, 112, 229-235.
Weidmann, U., 1993. Transporttechnik der Fussgänger. Tech. rep., Institutfür Verkehrsplanung und Transportsysteme, ETH Zürich, ETH-Hönggerberg, CH-8093 Zürich, in German.
Wikipedia, 2019. List of human stampedes. https://en.wikipedia.org/wiki/List_of_human_stampedes (Assessed on Mar 1, 2019).
Wong, S. C., Leung, W. L., Chan, S. H., Lam, W. H. K., 2010. Bidirectional pedestrian stream model with oblique intersecting angle. ASCE Journal of Transportation Engineering 136, 234-242.
Xiao, Y., et al., 2016. A pedestrian flow model considering the impact of local density: Voronoi diagram based heuristics approach. Transportation Research Part C 68, 566-580.

Xie, S., Wong, S. C., 2015. A Bayesian inference approach to the development of a multidirectional pedestrian stream model. Transportmetrica A, 11: 61-73.

Yanagisawa, D., Tomoeda, A., Nishinari, K., 2012. Improvement of pedestrian flow by slow rhythm. Physical Review E 85, 016111.

Yao, L., Sun, L., Zhang, Z., Wang, S., Rong, J., 2012. Research on the behavior characteristics of pedestrian crowd weaving flow in transport terminal. Mathematical Problems in Engineering, 2012, 264295.

Zhang, J., Klingsch, W., Schadschneider, A., Seyfried, A., 2011. Transitions in pedestrian fundamental diagrams of straight corridors and t-junctions. Journal of Statistical Mechanics, P06004.

Zhang, J., Klingsch, W., Schadschneider, A., Seyfried, A., 2012a. Ordering in bidirectional pedestrian flows and its influence on the fundamental diagram. Journal of Statistical Mechanics, P02002.

Zhang, X. L., Weng, W. G., Yuan, H. Y., 2012b. Empirical study of crowd behavior during a real mass event. Journal of Statistical Mechanics, P08012.

Zhang, J., Mehner, W., Holl, S., Boltes, M., Andresen, E., Shadschneider, A., Seyfried, A., 2014. Universal flow-density relation of single-file bicycle, pedestrian and car motion. Physics Letters A 378, 3274-3277.

Zhao, Y., Zhang, H. M., 2017. A unified follow-the-leader model for vehicle, bicycle and pedestrian traffic. Transportation Research Part B 105, 315-327.